

The Hatching-Box: A Novel System for Automated Monitoring and Quantification of *Drosophila melanogaster* Developmental Behavior

Julian Bigge^{1,2}, Maite Ogueta^{3*}, Luis Garcia^{1,3}, Benjamin Risse^{1,2*}

^{1*}Institute of Geoinformatics, University of Münster.

^{2*}Faculty of Mathematics & Computer Science, University of Münster.

^{3*}Institute of Neuro- and Behavioral Biology, University of Münster.

*Corresponding author(s). E-mail(s): m.ogueta@uni-muenster.de;

b.risse@uni-muenster.de;

Contributing authors: j.bigge@uni-muenster.de;

luis.garcia@uni-muenster.de;

Abstract

Drosophila melanogaster is among the most frequently used model organism in biology and life science as well as for development of novel treatments in the medical domain. In these fields, an analysis of behavioral patterns of the flies throughout their whole life cycle is of significant importance. For experimental purposes, large numbers of different *Drosophila* genotypes are cultivated in rearing vials and monitored for anomalies in their behavior or development, for example when exposed to stimuli or substances. From this, researchers are able to draw conclusions regarding the effect of the involved substances or treatments on humans, other animals or the environment. A major drawback of current state-of-the-art monitoring systems is the high amount of manual and time-consuming labor as most of the methods employed today require individualization of the flies or similar steps which prevents fully automated experiments. In this paper we propose the Hatching-Box, a novel imaging and analysis system to automatically monitor and quantify the developmental behavior of *Drosophila* in standard rearing vials and during regular rearing routines, rendering explicit experiments obsolete. This is achieved by combining custom tailored imaging hardware with dedicated detection and tracking algorithms, enabling the quantification of larvae, filled/empty pupae and flies over multiple days. Given the affordable and reproducible design of the Hatching-Box in combination with our generic client/server-based software, the system can easily be scaled to monitor an arbitrary amount of rearing vials simultaneously. We evaluated our system on

a curated image dataset comprising nearly 470,000 annotated objects and performed several studies on real world experiments. We successfully reproduced results from well-established circadian experiments by comparing the eclosion periods of wild type flies to the clock mutants per^{short} , per^{long} and per^0 without involvement of any manual labor. Furthermore we show, that the Hatching-Box is able to extract additional information about group behavior as well as to reconstruct the whole life-cycle of the individual specimens. These results not only demonstrate the applicability of our system for long-term experiments but also indicate its benefits for automated monitoring in the general cultivation process.

Keywords: Behavioural methods, Neuroscience, Machine Learning, Software

1 Main

The model organism *Drosophila melanogaster* has been used to study different aspects of biology, such as genetics, neuroscience or cell biology, and in recent years even for translational studies for human diseases [1, 2]. The whole life cycle of *Drosophila* comprises 4 different stages: egg, larvae, pupae and adults, and often it is of interest to know when and how many animals enter a specific developmental stage and how long they do remain in this stage. One commonly studied transition is the adult emergence or eclosion of *Drosophila*. In 1971, Konopka and Benzer found that this is time of day dependent and that mutations in a single gene named *period* affected this process [3]. The mutants they used do not only show a change on the timing of eclosion, but also show diverging pace in their development as a whole [4].

The study of eclosion is still a common procedure to study the circadian rhythms of the flies [5], as well as the developmental timing of pupation [6]. This type of experiments are time-consuming and often involve the constant personal monitoring of the rearing vials. Despite the growing necessity in various research domains, circadian experiments continue to be a challenging and time-consuming task to this day since the tools available either require fluorescent dyes to visually mark interesting brain regions [7] or extracting individual animals from their rearing vials and monitoring them in a distinctive system. An example of such a system is the commonly used Trikinetics Eclosion Monitor for which *Drosophila* pupae are glued to a disc and emerging adult flies fall down and are counted as they cross an infrared barrier [8]. Other, camera-based systems, record videos of the animals which can then be annotated semi-automatically by the experimenter with an imaging software such as Fiji [9–11]. For more detailed studies automated tracking systems have been developed which automatically extract the behavior of individual flies or larvae over time and were surveyed by Panadeiro et al. [12]. For example anTrax, Ctrax and Idtracker.ai are commonly used tracking applications that allow tracking of multiple *Drosophila* over a period of hours [13–15]. Providing a fine-tuned combination of a custom made imaging system and tracking software, Risse et al. proposed FIMTrack [16]. The proposed imaging hardware consists of an arena made from an acrylic glass plate which is illuminated by infrared LEDs using frustrated total internal reflection (FTIR) and

recorded with an infrared sensitive camera. This system was extended to be used for *Drosophila* larvae crawling in FTIR-illuminated rearing vials, yielding fine-grained 3-dimensional trajectories of the animals' movement [17]. Similarly for the domain of ethology Geissmann et al. designed an open source ethoscope system which can track adult flies [18] and analyze their behavior. Apart from methods focused on *Drosophila* there is also DeepLabCut which is often used for mice [19] but is also applicable for other animals including flies.

The aforementioned systems share considerable limitations and are often not directly applicable for long term experiments and lifelong monitoring as needed in circadian rhythm and other experiments. For example, anTrax, Ctrax, IdTracker.ai and DeepLabCut do not include specific imaging hardware which can cause difficulties in applying these software to custom imaging conditions and experimental setups. Moreover, identifying a suitable combination of cameras and recording software can have a significant influence on the performance of the tracking algorithms. Methods such as FIMTrack or the ethoscope combine software and adapted imaging hardware but still rely on an explicitly prepared and implemented experiments. The same also holds for the commercially available monitoring systems from Trikinetics, which only yields very basic activity information of the animals.

Another substantial constraint of these methods with regards to long-term behavior experiments is their inability to discriminate between different developmental stages of *Drosophila* which is a prerequisite to study the life cycle of flies. Since 2023, flyGear offers a commercially available system that can be used to classify *Drosophila* larvae and pupae, counts them and provides automatic data analysis and visualization [20–22].

To enable high-throughput, long-term (circadian) behavior experiments as well as automatic monitoring of *Drosophila* development during breeding, we propose an open-source system called *Hatching-Box*. Our system provides numerous advantages compared to current state-of-the-art: 1. Life-time monitoring of *Drosophila* is facilitated in off-the-shelf rearing vials during the conventional rearing routine. As a consequence, our system does not require the manual collection of animals and no preparation of the tracking system is necessary, enabling behavioral quantifications without any labor overhead. 2. Each system houses up to three rearing vials (41.5mm diameter), can be placed in incubators or cultivation rooms and comprises primarily off-the-shelf hardware components with some 3D printed and manufactured parts from easily obtainable materials so that an arbitrary amount of stackable monitoring systems can run in parallel. 3. The self-contained hardware design renders the internal imaging modalities independent from external influences. Hence, the hardware, firmware and software are precisely aligned to fit this setup to yield accurate and reproducible results. 4. A machine learning-based object detection algorithm based on YOLO is adapted and trained on nearly 470.000 manually labeled objects. Our system is capable of accurately detecting all developmental stages of *Drosophila* even in very cluttered conditions, yielding an accuracy of up to 91% while providing real-time processing capabilities. 5. An array of built-in sensors is integrated to monitor the temperature and humidity within each box. In addition, dedicated light stimulation has been integrated, which can either automatically adapt the inner lighting conditions

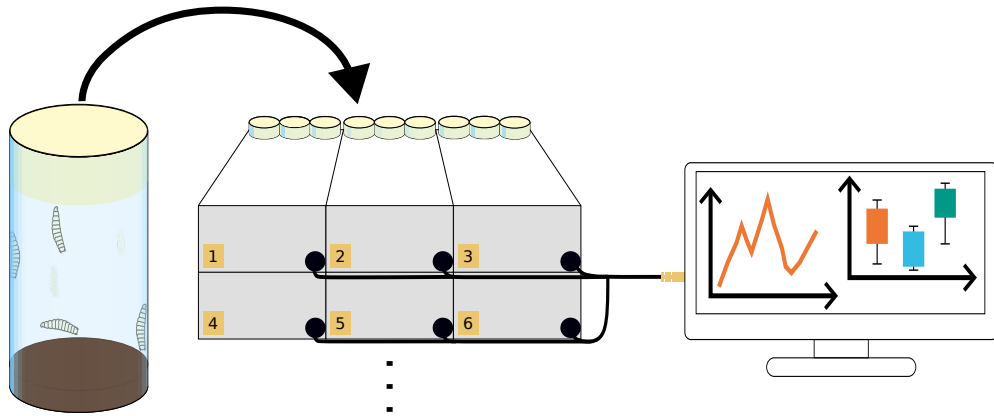


Fig. 1: System overview showing stackable Hatching-Boxes. Standardized rearing vials used to house *Drosophila* can be placed in the Hatching-Box, which then automatically tracks the population’s behavior and provides images and behavior analysis to a central computer.

to the external brightness or can be programmed to provide individual illumination schemes for each box. 6. We implemented an easy-to-use GUI that can be used for controlling the camera, start or stop a recording and automatically analyze the data. 7. All components (i.e. hardware, firmware, software) have been tested and a rigorous evaluation of our system was conducted by reproducing the results of Konopka and Benzer in a well-established circadian experiment by using the three *Drosophila* clock mutants *per^{short}*, *per^{long}* and *per⁰* and comparing their activity cycles with the wild type. 8. The full source code, collected dataset, a conclusive bill of materials and required files for the 3D printed and manufactured parts will be made available under an open-source license.

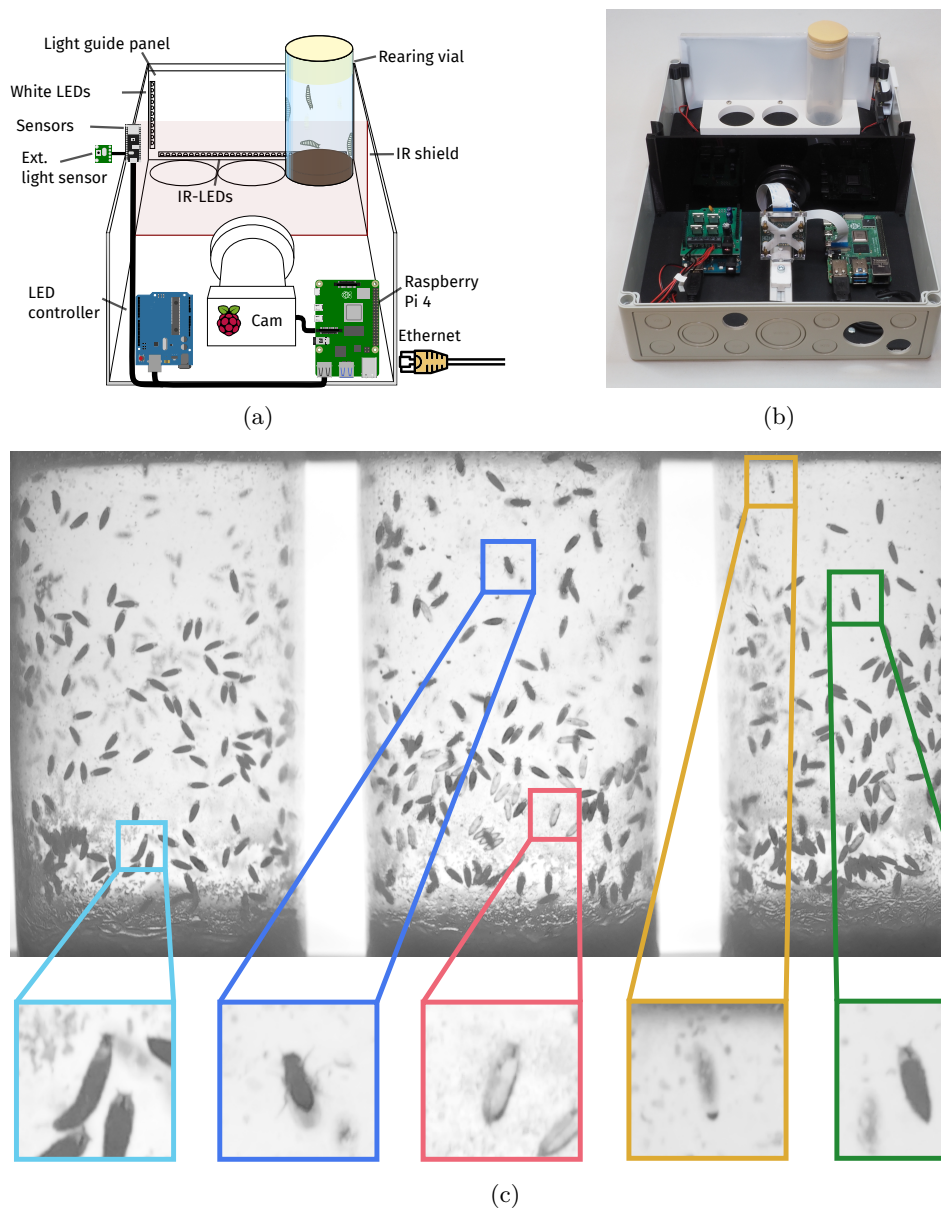


Fig. 2: Overview of the proposed hardware architecture. (a) A single Hatching-Box consists of a RaspberryPi 4 with the HQ camera module, an LED controller device (Arduino Uno + custom shield), an Arduino Sense BLE 33 sensor board, as well as a light guide panel, outfitted with IR and white LEDs. (b) Picture of a Hatching-Box with cover removed. (c) Image as taken by our Hatching-Box with different objects highlighted: third instar larva (cyan), adult fly (blue), empty pupa (red), out-of-focus (yellow) and full pupa (green).

2 Results

2.1 Hardware

The hardware of our system is designed to be easily integrated into established daily laboratory routines to provide long-term monitoring capabilities without the need for additional manual labor. This requires the use of rearing vials for animal housing and a small overall footprint of the system to fit into most incubators. While we use rearing vials with a 41.5mm diameter, our system can be easily adapted to other vials as well by editing one of the provided parametric manufacturing files (see Appendix B). Additional sensors and light sources provide supervision and control over the breeding conditions in each box. We use a standard small-sized plastic electrical box for the main compartment, housing our central computing device, a Raspberry Pi 4, a camera and additional necessary technical components and up to three standard rearing vials (see Figure 2a). The form factor of these boxes enable arbitrary stacking of multiple setups for high-throughput experiments and each box is individually connected via Ethernet to operate several systems in parallel (see Figure 1). The built in camera captures frames using a user-specified frame rate allowing for continuous recordings or time-lapse sequences. For illumination an acrylic based light guide panel is positioned behind the rearing vials which is equipped with several near infrared and white light-emitting diodes (LEDs). In order to visually detect small and semi-translucent objects (e.g. empty pupae, larvae, etc.) we optimized the transmitted light configuration by deriving a custom diffusion pattern, providing homogeneous diffuse illumination across the light guide panel (see Appendix D). The IR LEDs are used for image capturing only given this wavelength is reported to be invisible for flies [23]. An additional IR shield in the middle of the compartment prevents light emitted by the computing hardware to have an influence on the specimens or produce reflections on the rearing vials. We synchronized the IR LED activation with the camera so that IR light is only present during image acquisition while being turned off otherwise to prevent heat buildup and to keep a low energy profile (see Sec. 4.1.3). Temperature and humidity sensors inside each box record temporally synchronized measures of the breeding conditions. The white LEDs provide a visual stimuli and can either be freely programmed for each box individually or can be synchronized with the outside brightness using an externally mounted brightness sensor (e.g. to mimic the lightning conditions of the surrounding incubator; see Sec. 4.1.3). The combination of the high resolution camera and the optimized backlight panel yield detailed images of all developmental stages of *Drosophila* (see Figure 2c) which are subsequently used for data collection and in our classification and tracking pipeline.

2.2 Dataset

For training our YOLOv7 object detector we curated a dataset containing *Drosophila* in various developmental stages, i.e. *larva*, *pupa*, *empty pupa*, *adult fly*. In addition we marked out-of-focus objects on the backside of the vials since these blurred objects can be the cause of misdetections and misclassifications. In total we annotated 469,120 objects (bounding boxes and class labels) in 1505 images recorded in

different Hatching-Box systems. The first 200 images were labelled thoroughly by domain experts. We utilized these first images to train an initial YOLOv7-E6E model which was subsequently used to provide suggestions to the annotators to speed up the labeling process. Importantly, all suggestions proposed by our model were manually checked by domain experts. Table 3b shows the class distribution across our dataset.

2.3 Software

2.3.1 Detection and classification of *Drosophila* using YOLOv7

Detection and classification (distinguishing different developmental stages of *Drosophila*) in the images captured by our system is performed by the YOLOv7 machine learning model [24]. YOLOv7 provides various versions, i.e. the base model, -tiny, -X, -E6, -W6 and -E6E, comprising different depth of scaling pyramids helping to detect smaller objects in exchange for higher parameter count and compute overhead. We trained these models on our curated dataset (see Sec. 2.2) with the same train-validation split (80:20) for 300 epochs and compared their performance on the validation dataset. In our experiments we found that for the task of detection and classification of *Drosophila* in our Hatching-Box images, the different model variants show comparable performance with regards to their classification accuracy. The best performing model shows 4.35% better mAP on 50% to 95% IoU compared to our YOLOv7-tiny baseline, while it only shows a surplus of 0.73% in mAP on 50% IoU (see Figure 3). However, deep scaling pyramids as supplied by the larger YOLOv7 models (E6, W6, E6E) are not shown to be beneficial for overall classification performance. Additionally, we can observe a small decrease in AP compared to the other models which we trace back to slight overfitting on our training data.

We also evaluated class confusion for our model to evaluate its ability in recognizing different *Drosophila* developmental stages (Fig. 3f). Specifically, full and empty pupae are detected with a 95% and 97% accuracy and are only occasionally confused with each other. Adult *Drosophila* are correctly detected in 86% of the cases, in 12% of the cases the fly is detected incorrectly as an out-of-focus object which can be explained by their ability to freely move in the vial compared to larvae and pupae, escaping the focal plane of the camera. Similarly, detection of larvae shows a 84% accuracy, most commonly confused with full pupae (8%), since these two classes have a similar appearance in single channel grayscale IR images. As can be seen in the confusion matrix our models successfully differentiates between *Drosophila* and environmental clutter: only 1% of adult flies and (full/empty) pupae and only 3% of larvae are misclassified as background (background false negatives). Conversely, in the case a background object is detected as a foreground object (background false positives), it is discarded as the out-of-focus class in 63% of the time. Over the course of the performed experiments, our detection algorithm identified up to 500 unique specimens per image. As a direct result of our high-throughput system, single misdetections on a frame-by-frame basis can statistically be compensated on a frame-by-frame basis. We achieve additional robustness for the detections by implementing a temporal association mechanism which takes multiple previous reference time points into account to produce a most probable identity matching over a whole image sequence.

2.3.2 Identity preserving tracking

As mentioned above, YOLOv7 provides detections (bounding boxes) surrounding the foreground objects and associated class labels, namely adult fly, filled pupae, empty pupae, larvae and out-of-focus object. The former four object types are subsequently used in an identity preserving tracking algorithm to compute continuous trajectories for all individuals over time (see Sec. 4.2.4). By jointly considering the bounding box location and area as well as the object class, temporal association of a box at time t and $t - 1$ requires an IoU of more than 60% and the same or adjacent developmental stages between two consecutive frames. In addition, temporal smoothing is used by integrating multiple past frames which also enables the preservation of identities in case of occasionally missed detections (e.g. due to object occlusions). For our scenario a time window of three additional frames at $t - 2$, $t - 3$ and $t - 4$ yielded good results.

During our circadian experiment (Sec. 2.3.3) we have captured with a framerate of one frame each 10 minutes to reduce the amount of accumulated data. This is sufficient to detect pupation and eclosion events in the lifecycle of *Drosophila*, used as indicator for their circadian rhythm, as the specimens stay immobile during the pupal stage and therefore do not move inbetween frames. Additionally, recording with the current maximum framerate of 1 fps, our system is also able to track larvae locomotion (see Fig. 4). In contrast, tracking of fast moving adult flies would require a significantly higher framerate which was not tested during the course of the experiment, albeit technically supported.

Life-long monitoring and complex experimental settings require recordings over multiple weeks resulting in thousands of trajectories. However, these also include trajectories that only cover a small number of frames, usually occurring for adult *Drosophila* that can move particularly fast when flying and hence cannot be tracked using the aforementioned frame rate. Given our focus on the transitions in developmental stages we discarded small trajectories below 30 consecutive detections.

To assess the performance of our tracking pipeline we measured the average computation required for tracking a random sequence of 100 consecutive frames of a video of ten runs with each of the previously introduced YOLOv7 models as a detector (see Fig. 3). We compare the time the YOLOv7 model needs for inference and the time required for temporal association as introduced in this section on an AMD Ryzen 7 3700X 8-Core CPU and a NVIDIA GeForce RTX 3060 Ti GPU. On average, each frame of the selected random sequence has around 500 detected objects (out-of-focus objects excluded) that have to be associated between consecutive frames. Nevertheless, when run on the CPU, the average overhead of our tracking algorithm compared with only inference of the YOLOv7 models was between 112.28 and 136.52 ms. For the basic, less resource intensive YOLOv7-tiny, the temporal association algorithm on average constitutes 24.7% of the overall runtime per frame. When used with the most complex YOLOv7 model, YOLOv7-E6E, the share of total runtime decreases to only 2.3%. A similar distribution can be observed when our pipeline is employed on a system with a GPU, even though the average processing time of the temporal association is a bit higher between 134.54 and 154.11 ms. This amounts to an 48.0% share of runtime when used with YOLOv7-tiny compared to 28.7% when used with YOLOv7-E6E.

In a second step of our postprocessing routine we apply a centered median filter of size five to the associated developmental stage at each point in time for each individual specimen. This way, our tracker filters out single misclassifications that can appear on a frame-by-frame basis due to different factors, e.g. another object covers up the specimen or during the process of a larva pupating. Subsequently, after postprocessing, the determined positions and developmental stages over the time of the experiment for each specimen is saved in an output file in HDF5 that can directly be converted to be used for analysis in other established frameworks such as rhetomics [25] (see Sec. 2.3.3) or custom analysis scripts.

2.3.3 Performance evaluation

To assess the performance of the Hatching-Box, we performed experiments with four different genotypes, a wild type line *iso31* [26] and the three well-known mutants for the period of emergence of adult flies [27]: *per^{short}*, *per^{long}*, *per⁰*. While wild type flies have a period of eclosion of about 24 hours in constant darkness, this behavior can be affected by mutations of the *period* gene. *per^{short}* flies show an eclosion period of 19h, *per^{long}* change it to 26h and *per⁰* fail to form a rhythmic pattern.

The experiments were performed in a temperature controlled incubator (CLF, Plant Climatics) set at 25°C, in constant darkness to be able to study the inner rhythm of the flies without effect of the light. We monitored three vials of each genotype per Hatching-Box with a image capturing interval of 10 minutes and configured the tracker to only track full and empty pupae. With this configuration we monitored the different genotypes for 14 days each and computed the quantitative results as described in Sec. 2.3.2. To find the time points of eclosion/pupation based on this output we processed the sequence of detected developmental stages for each separate specimen with a sliding window of size τ (with $\tau = 7$ for our framerate). We mark a time point t as time of eclosion/pupation if a majority of time points $[t, \dots, t + \tau - 1]$ are associated with the class of empty/full pupa. For the performed circadian experiments we used this approach to extract the eclosion time points only.

In Fig. 5 we can observe in the diagrams that at the beginning there is no eclosion, as expected, since most of the animals are in the stage of larvae. At about day 4-5 we start observing an increasing number of events. The *iso31* flies show a rhythm of 24 hours as expected, that is also detected in the periodogram, while in the *per⁰* there is no clear rhythm. The *per^{long}* flies show a rhythm of 28.3 h, and interestingly, the beginning of the eclosion is delayed compared to the other genotypes. Lastly, even though the periodogram of *per^{short}* flies does not show any significant rhythm, it can be recognized in the actogram a short rhythm that is also detectable in the periodogram of about 19h, that would represent the published data.

3 Discussion

Extracting large quantities of developmental and behavioral data is essential for a variety of biological experiments. However, the acquisition of this type of data involves tedious and time-consuming labor, aggravating the reproducibility and limiting the throughput. This predicament builds momentum for the emergence of automated

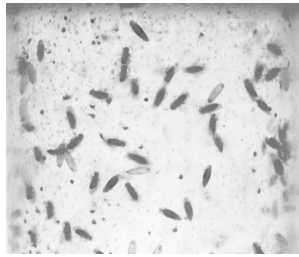
Model	AP ^{val}	AR ^{val}	mAP ₅₀ ^{val}	mAP _{50:95} ^{val}	Class	Count	Share
YOLOv7-tiny	91.93%	90.01%	93.28%	73.03%	Empty Pupa	147,886	31.52 %
YOLOv7-X	91.29%	89.84%	92.91%	75.39%	Out-of-focus	143,084	30.50 %
YOLOv7	91.65%	90.27%	93.23%	74.87%	Full Pupa	105,923	22.58 %
YOLOv7-E6	91.69%	90.06%	93.62%	77.16%	Adult Fly	46,520	9.92 %
YOLOv7-W6	91.23%	89.62%	94.01%	77.38%	Larva	25,707	5.48 %
YOLOv7-E6E	90.55%	90.05%	93.27%	76.35%	Total	469,120	

(a)

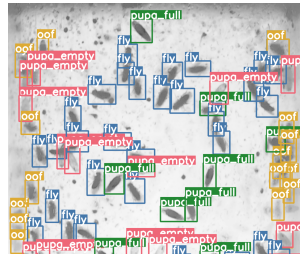
(b)

	Model	Inference		Tracking		Overall	
CPU	YOLOv7-tiny	438.69	(±21.94)	132.79	(±19.27)	611.31	(±27.63)
	YOLOv7-X	5240.78	(±90.83)	112.28	(±15.03)	5393.07	(±91.19)
	YOLOv7	3162.86	(±70.04)	120.23	(±16.02)	3323.05	(±69.99)
	YOLOv7-E6	3639.89	(±79.95)	132.93	(±19.61)	3812.84	(±80.40)
	YOLOv7-W6	2328.11	(±59.51)	129.02	(±18.09)	2497.16	(±58.69)
YOLOv7-E6E	5718.86	(±104.26)	136.52	(±21.87)	5895.45	(±104.78)	
GPU	YOLOv7-tiny	133.12	(±4.62)	160.87	(±17.33)	335.72	(±16.86)
	YOLOv7-X	336.64	(±6.19)	135.90	(±12.56)	514.65	(±12.47)
	YOLOv7	243.77	(±4.76)	144.87	(±13.09)	430.83	(±13.24)
	YOLOv7-E6	271.81	(±6.20)	162.68	(±17.25)	476.60	(±16.76)
	YOLOv7-W6	211.72	(±4.02)	157.63	(±15.41)	411.47	(±15.47)
YOLOv7-E6E	370.27	(±6.13)	165.77	(±20.87)	578.25	(±19.98)	

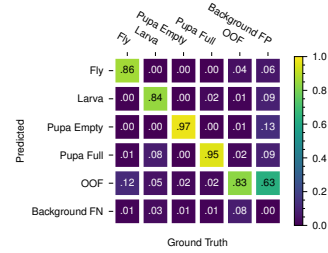
(c)



(d)

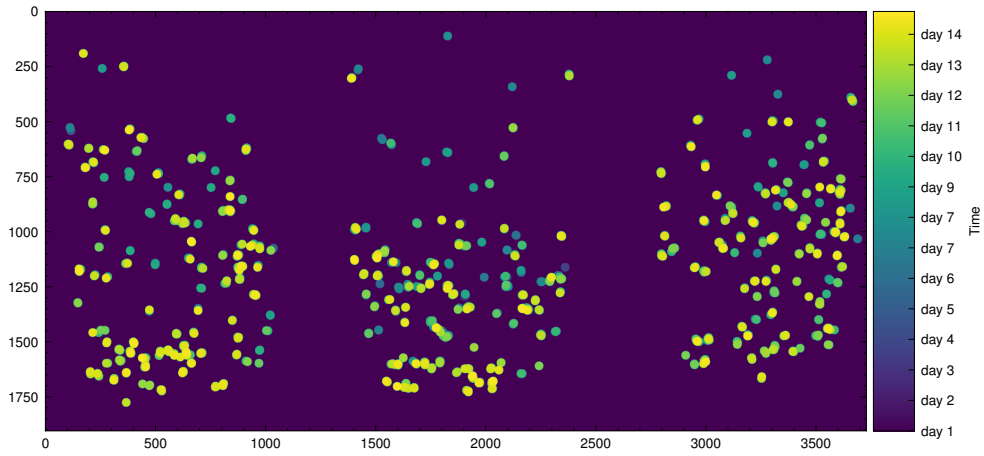


(e)

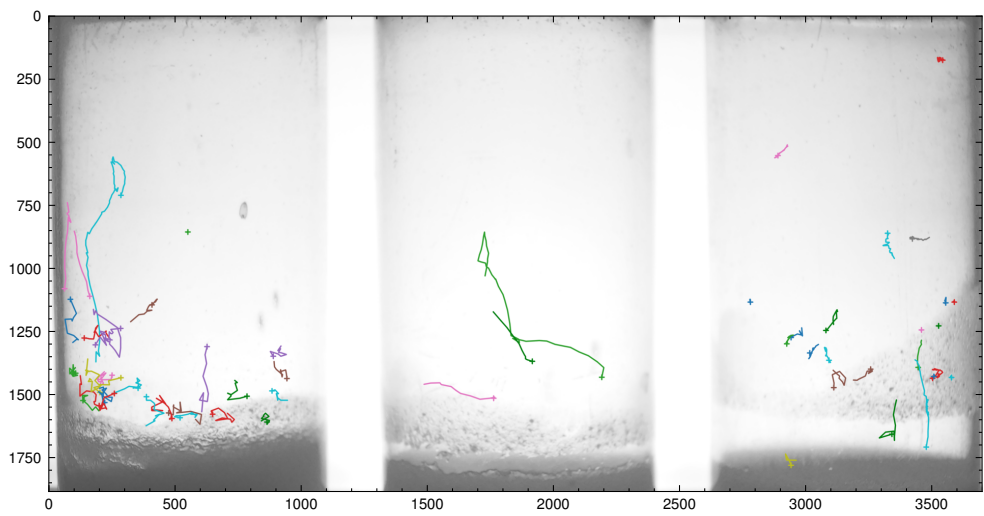


(f)

Fig. 3: (a), Comparison of average precision (AP), average recall (AR) and mean average precision (mAP) of the YOLOv7 models trained on our Hatching-Box dataset (out-of-focus objects excluded). (b), Overview of the class distribution of our curated dataset. (c), Average inference and tracking time comparison in ms/frame on a CPU (AMD Ryzen 7 3700X 8-Core) and GPU (NVIDIA GeForce RTX 3060 Ti). (d),(e), Crop of an image as taken with our system before and after object detection by YOLOv7. The detected objects are third instar larvae (cyan), adult flies (blue), empty pupae (red), full pupae (green) and out-of-focus (yellow). (f), Class confusion matrix of the used YOLOv7-tiny model. (For full comparison see Appendix A)



(a)



(b)

Fig. 4: (a), Positions of eclosion (wildtype *Drosophila*) over the course of our 14 days circadian experiment. (b), Larva locomotion (wildtype *Drosophila*) over 100 second captured with our system with 1 fps.

hard- and software solutions to aid researchers gain new insights, e.g., in the field of neurosciences [29] and genetics [30]. However, the shift towards higher automatization also imposes new challenges and limitations which restrict the number of specimens that can be monitored and the length of the supported observation period. Most available systems focus on high temporal and spatial resolution when tracking behavioral

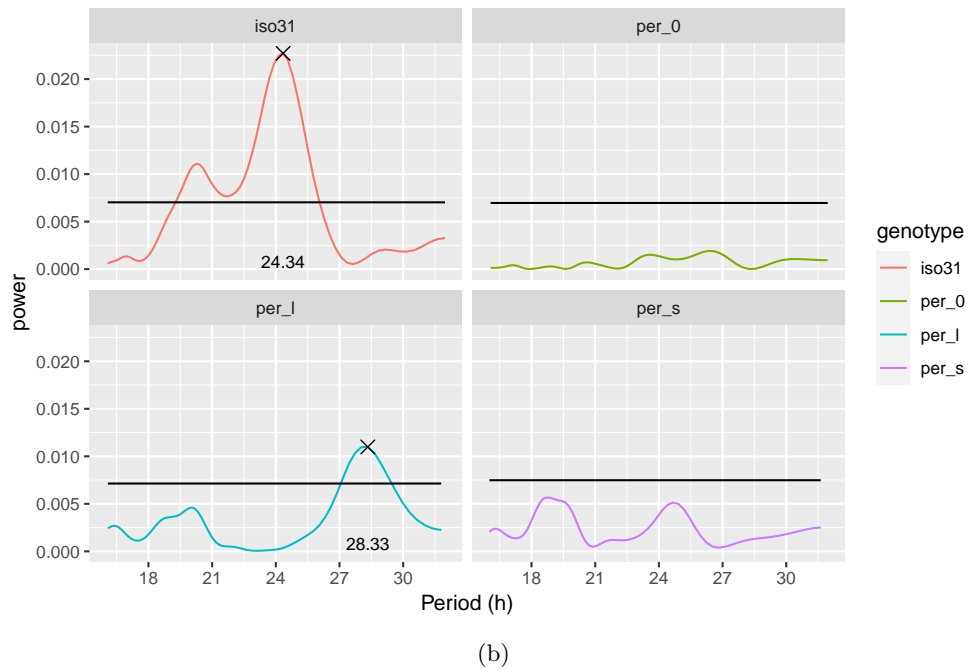
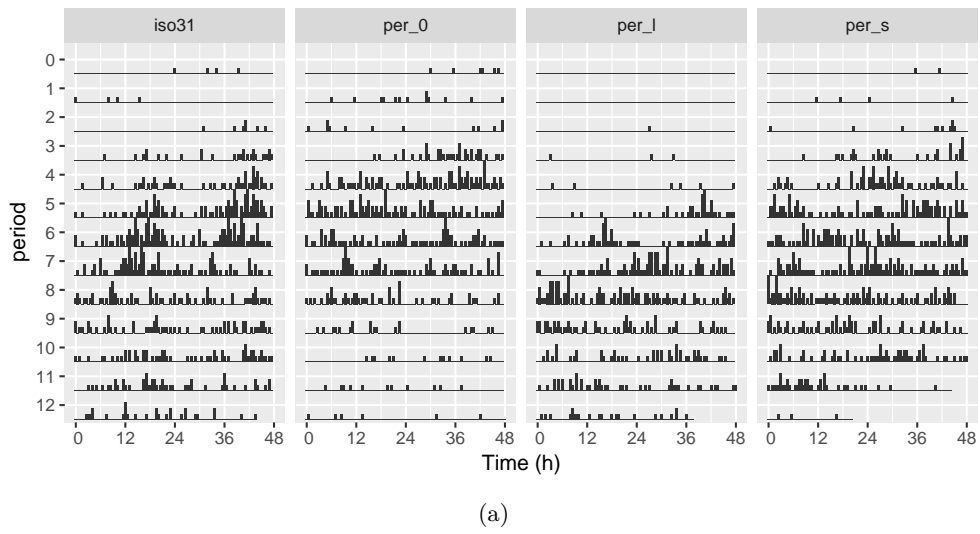


Fig. 5: Comparison of periodicity of selected clock mutants per^0 , per^{short} , per^{long} and wildtype $iso31$ as recognized by the Hatching-Box. We used the statistical methods of the R package *rhetomics*. (a), Double plotted actogram of eclosion events for the different genotypes. (b), Lomb-Scargle periodogram of observed mutants [28].

features of animals such as their movement which renders them inappropriate for the analysis of long-term experiments or population development.

In this paper we have introduced an alternative tracking approach for long-term experiments. Our hardware and software combinations offers fully automatic developmental and behavioral quantifications, which are integrated into the regular rearing process, hence do not require any additional labor. The machine learning-based object detection and tracking algorithm enable the quantification of short larval trajectories, pupation and eclosion including their rhythmicity and temporal development as well as rudimentary activity monitoring. By making the exhaustive tracking data available as an HDF5 file, we additionally encourage further analysis of the collected data with tools and frameworks already established by the user. The cost-effective and easy to build hardware, as well as the client-server-based software allow for arbitrary extensions yielding highly parallelized and high-throughput screenings.

The software is developed with a particular focus on throughput to detect, classify and track specimens in the captured images over the whole course of the experiment without manual intervention. The combination of these different components result in high quality tracking results for experiments with hundreds of animals spanning multiple weeks that are not straightforward to acquire with software-only tracking solutions (e.g. [15, 19]) which require the experimenter to establish an appropriate imaging setup. The presence of user-controllable lights within each Hatching-Box facilitates multiple experiments with different light cycles in the same incubator. Additionally, by utilizing our sensor array, the environmental conditions during the experiment can be closely monitored and easily correlated with the obtained developmental data. Being able to track *Drosophila* in their rearing vials takes the burden off of experimenters to individualize their specimen and simultaneously makes the Hatching-Box also applicable for monitoring of their general development and gathering behavioral and fitness features on-the-fly.

Given our approach favors high throughput over fine-grain behavioral feature extraction, this introduces new challenges regarding identification of objects inside the rearing vials. On the one hand, off-the-shelf rearing vials are usually made of plastic, e.g., polypropylene, that is not as transparent as acrylic glass or certain other plastics depending on material quality which can complicate detection of animals. On the other hand, achieving a focal plane depth adequate for distinguishing animals in the cylindrical housing is not a trivial task. We mitigated this issue by choosing the focal depth in a way that objects in the camera-facing front of the rearing vial appear sharp and any other objects blurred so that foreground and background objects can be readily differentiated. Still, both the aforementioned factors can contribute to erroneous detections and classification suggested by the YOLOv7 model. Nevertheless, our experimental results show that we are able to mitigate this issue by usage of our postprocessing routines which ultimately produce continuous trajectories even if detections are missing or inaccurate on a frame-by-frame basis.

In the future, we will integrate a vibration-free rotation mechanism for the rearing vials to further increase the total number of observable objects.

Due to framerate limitations of up to 1 frame per second (fps) when using the full 12 megapixel resolution of the camera module, our current implementation does

not achieve a sufficient temporal resolution to track flying adult flies. We aim on further increasing the framerate to ultimately also allow behavioural analysis of fast moving specimen. This may pose further challenges, e.g., additional heat buildup and throughput limitations of the local network, which may involve modification of the current software architecture.

4 Methods

4.1 Hardware

4.1.1 Hardware Design

As the main compartment for our system we used an off-the-shelf electrical box measuring 355.0mm \times 248.0mm \times 110.7mm (*length \times width \times height*), providing enough room for the necessary electrical components as well as three rearing vials with a diameter of 41.5mm (see Appendix C). For our system we employed an adapted set of imaging components, backlight illumination and additional sensors as specified below (see Appendix B).

4.1.2 Imaging components

Image recording is performed with the Raspberry Pi High Quality Camera module connected to the Raspberry Pi 4 (8 GB). The camera module uses the 12.3 megapixel Sony IMX477 sensor and is equipped with a C/CS mount which provides compatibility with a large number of camera lenses. When the camera is used with its full resolution of 4056 \times 3040 pixels, our system can achieve a frame rate of up to 1 frame per second. For our experiments we used the C125-0818-5M Basler lens with 8mm focal length due to its minimal working distance (MOD) of 100mm. We outfitted the lens with a MIDOPT LP818-46 low-pass IR filter with a useful range of 825nm - 1100nm. The builtin IR block filter of the camera module was removed. Additionally

4.1.3 Backlight illumination

Since the lighting conditions of an image have a significant influence on its characteristics and in turn on the performance of object detection algorithms we also propose a custom light guide panel design for the Hatching-Box. Our light guide panel is made of acrylic glass with punctures on the surface, distributing the incoming light homogeneously across its area.

The Hatching-Box uses two separate light sources. The first one consists of two LED strips emitting white light (250nm - 800nm) and can be used as a stimulus for the monitored *Drosophila*. A second LED strip consists of IR LEDs with a wavelength of 890nm has been placed at the bottom edge of the light guide panel behind the rearing vial holder to provide a homogeneous illumination across its entire area. As a driver for the LEDs in our system, we use a standard Arduino Uno in combination with a custom-made shield that is connected to the Arduino's GPIO pins [31]. In their publication, Ogueta et al. used LED strips with four color channels red, green, blue and white (RGBW) which are connected to the shield. In our implementation we use

three of these four channels for controlling the the two white LED strips and the IR LED strip independently.

4.1.4 Sensors

Environmental conditions play a significant role for breeding and experimental designs. We therefore equipped the Hatching-Box with sensors for temperature and humidity (HS3003), light intensity (APDS9960) and barometric pressure (LPS22HB), all provided by the Arduino Sense BLE 33 sensor board. As an external digital light sensor to measure brightness outside of the Hatching-Box we use a BH1750. We implemented a custom-made firmware to query the Arduino Sense via serial connection which automatically provides all current measurements every time an image is taken and saved in the experiment’s output HDF5 file.

4.2 Software

4.2.1 Overview

Our software architecture consists of two main components, namely the headless Hatching-Box client application (HB-client) executed on the Raspberry Pi on each box independently and the Hatching-Box server application (HB-server), designed to be used on a central computer (see Figure 6). The HB-client controls the camera and lights of the Hatching-Box and provides access to the integrated sensor board (see Sec. 4.1 for more details). On the other hand, the HB-server is executed on a computer connected to one or many Hatching-Box systems and provides an easy-to-use graphical user interface to control the capture modalities of each box. Moreover, the HB-server provides tools for long-term tracking and behavioral analysis of individual *Drosophila* specimen. For the purpose of communication, each Hatching-Box must be connected to the same network used by the server. Transmission of controls, images and other data is performed by a TCP/IP-based application protocol. By building our distributed architecture upon standard network protocols, our system can easily be extended or integrated into existing infrastructure.

4.2.2 Client architecture: HB-client

In our proposed architecture, the term “client” corresponds to an individual Hatching-Box (see Sec. 4.1). The soft- and hardware of each Hatching-Box is controlled by a Raspberry Pi 4. The Raspberry Pi is connected to a Raspberry Pi HQ camera module and, via USB, to an Arduino Sense BLE 33 sensor board which are used for capturing images and sensor data respectively. As a driver for the camera, the HB-client uses the libcamera software stack [32]. Libcamera enables control of the camera’s recording parameters, e.g. exposure time and analog/digital gain, and construction of an image processing pipeline that uses firmware-based image processing in combination with custom-made processing routines. This processing includes routines for isolating a region of interest (ROI) from the captured image as well as detecting the boundaries of each monitored vial to support experimental designs which require observing different classes such as varying phenotypes. The parameters of the processing steps can be

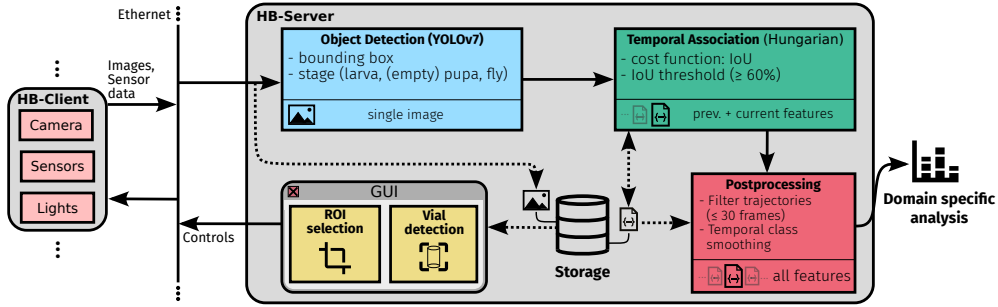


Fig. 6: Overview of data and command flow in our proposed system’s architecture.

controlled in the HB-server application (see Sec. 4.2.3). Images are recorded using the BGR888 pixel format, encoded and compressed in PNG format and subsequently sent to the server. The LED controller, also connected via USB, is specifically designed for circadian experiments and operates the backlight panel. The connected LED strips with different wavelengths (here: white and IR LEDs) can be controlled separately. The HB-client is launched automatically upon startup of the Raspberry Pi and first initializes the serial communication channels to the sensor board, the LED controller and the libcamera software-stack. After initialization, the HB-client connects to the configured IP address and port of the HB-server. Afterwards, the Hatching-Box maintains the connection to the server, reconnects if necessary, and idles until the user issues a snapshot/recording task, changes camera settings or until the next scheduled video frame has to be captured and transmitted. By transferring the recorded images directly to the server, we are able to fully omit write operations to the micro SD card, preventing data corruption.

4.2.3 Server architecture: HB-server

Following our architecture’s naming scheme, the “server” is represented by a single, off-the-shelf computer, preferably with a GPU, which executes the HB-server application. The HB-server consists of three main components: 1. a TCP server, 2. a graphical user interface (GUI) and 3. an object tracker (see Figure 6).

For TCP communication the HB-server builds on the ZeroMQ library [33] to maintain reliable, scalable and concurrent network connections to each Hatching-Box simultaneously while minimizing the overhead.

The HB-server uses the Qt5 framework to provide a graphical user interface (GUI) to supervise and coordinate experiments. All online Hatching-Boxes in the same network are enumerated by its time of connection and accessible in the GUI. By selecting an individual Hatching-Box, users can control recording parameters and define a region of interest to select specific vials to be monitored by the system. Previously recorded images and sensor readings (temperature, humidity, air pressure, light intensity and color) of the individual box can be reviewed. Multiple Hatching-Boxes and their adjusted settings can be organized in a *workspace*, which can be saved and then reused at a later time.

4.2.4 Tracking

To analyse the images recorded by the HB-client we implemented an adapted tracking algorithm, which is accessible in the HB-server. This algorithm firstly separates the image into individual rearing vial crops using a one-time calibration step, which automatically generates a mask for each vial (see Appendix E). The subsequent tracker pipeline consists of two main steps: 1. detection and classification of objects in the crops over time and 2. association of the detected objects over time to compute consistent identities. Detection and classification is done by the YOLOv7 framework, which has been used successfully on a wide range of domains including tiny insect detection [34] and medical imaging [35] and requires only moderate computing capabilities. For our experiments in Sec. 2 we used the baseline YOLOv7 model pretrained on the COCO dataset [36] and finetuned it on our custom Hatching-Box dataset (see Sec. 2.2). Loading and inference of our model is performed using the ONNX [37] framework to make use of platform-dependent acceleration methods. This decreases the inference time and provides an interface which makes it possible to also load other models to use in HB-server if desired. To further speed up the inference and the tracking process off-the-shelf GPU computing hardware is recommended.

The second step of our tracker is concerned with the temporal association and identity conservation in time. Assuming slow / non-moving objects (larvae or pupae) or an appropriate frame rate, the intersection-over-union (IoU) of bounding boxes of consecutive frames can be used as a metric for temporal association. The IoU of two bounding boxes b_i and b_j is defined by

$$J(b_i, b_j) = \frac{|b_i \cap b_j|}{|b_i \cup b_j|}. \quad (1)$$

Based on the pairwise IoU values of all bounding boxes in frame t , b_i^t ($i = 1, \dots, m$), and bounding boxes b_j^{t+1} ($j = 1, \dots, n$) in the subsequent frame, we construct $I_{t,t+1} \in \mathbb{R}^{m \times n}$ such that

$$I_{t,t+1}(i, j) = J(b_i^t, b_j^{t+1}). \quad (2)$$

We use the hungarian algorithm [38] to find a bijective mapping between the bounding boxes in frame t and frame $t + 1$ that maximizes

$$\sum_{i=1}^m \sum_{j=1}^n I_{t,t+1}(i, j). \quad (3)$$

To also allow detections that have no correspondence across both frames, additional n rows and m columns of dummy entries are added to $I_{t,t+1}$ to allow addition/deletion

of objects over time. This is [39]. The resulting matrix $I_{t,t+1}$ has shape $n + m \times m + n$:

$$I_{t,t+1} = \left(\begin{array}{cccc|ccc} J(b_1^t, b_1^{t+1}) & J(b_1^t, b_2^{t+1}) & \dots & J(b_1^t, b_n^t) & 1 & \dots & 1 \\ J(b_2^t, b_1^{t+1}) & J(b_2^t, b_2^{t+1}) & \dots & J(b_2^t, b_n^t) & 1 & \dots & 1 \\ \vdots & \vdots & \ddots & \vdots & \vdots & \ddots & \vdots \\ J(b_m^t, b_1^{t+1}) & J(b_m^t, b_2^{t+1}) & \dots & J(b_m^t, b_n^t) & 1 & \dots & 1 \\ \hline 1 & 1 & \dots & 1 & 0 & \dots & 0 \\ \vdots & \vdots & \ddots & \vdots & \vdots & \ddots & \vdots \\ 1 & 1 & \dots & 1 & 0 & \dots & 0 \end{array} \right) \quad (4)$$

Matching dummy objects with each other is prevented by setting $I_{t,t+1}(i, j) = 0$ for $m < i \leq m + n$ and $n < j \leq n + m$. Detected objects can be shown as an overlay on top of the captured images in the HB-server GUI.

4.3 Circadian Experiment

About 30 males and 30 females were crosses and their eggs collected in three vials (41.5mm diameter) with standard yeast-containing fly food and kept at 25C in a 12h : 12h light-dark cycles. The same parental flies were flipped twice, each time after 2 days of egg laying. The 4 genotypes used here (*iso31*, *per^{short}*, *per^{long}* and *per⁰*) have been described previously ([26, 27]). A set of three vials of the same genotype were tested simultaneously in the Hatching Box. The experiment was performed at 25C in a temperature controlled incubator (CLF, Plant Climatics) in constant darkness.

References

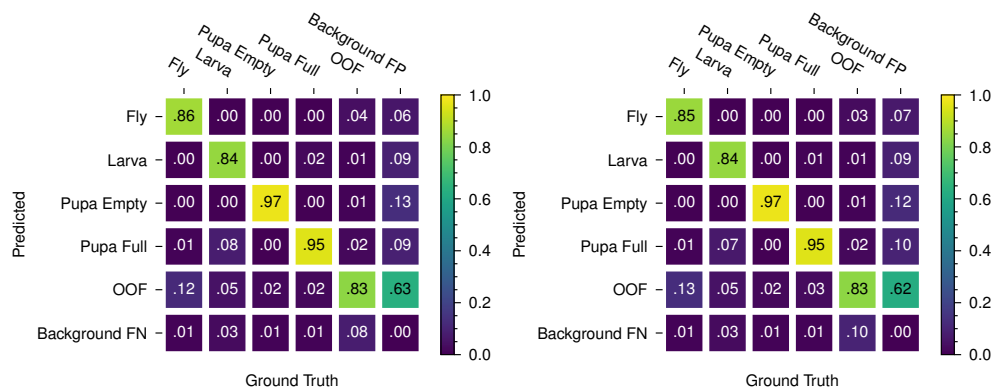
- [1] Tanaka, T. & Chung, H.-L. Exploiting fly models to investigate rare human neurological disorders. *Neural Regeneration Research* **20**, 21–28 (2025).
- [2] Dorkenwald, S. *et al.* Neuronal wiring diagram of an adult brain. *Nature* **634**, 124–138 (2024).
- [3] Konopka, R. J. & Benzer, S. Clock Mutants of *Drosophila melanogaster*. *Proceedings of the National Academy of Sciences* **68**, 2112–2116 (1971). Publisher: National Academy of Sciences Section: Biological Sciences: Genetics.
- [4] Kyriacou, C., Oldroyd, M., Wood, J., Sharp, M. & Hill, M. Clock mutations alter developmental timing in *drosophila*. *Heredity* **64**, 395–401 (1990).
- [5] Wegener, C., Amini, E., Cavieres-Lepe, J. & Ewer, J. Neuronal and endocrine mechanisms underlying the circadian gating of eclosion: insights from *drosophila*. *Current Opinion in Insect Science* 101286 (2024).
- [6] Juarez-Carreno, S. *et al.* Body-fat sensor triggers ribosome maturation in the steroidogenic gland to initiate sexual maturation in *drosophila*. *Cell Reports* **37** (2021).

- [7] Vallejo, D. M., Juarez-Carreño, S., Bolivar, J., Morante, J. & Dominguez, M. A brain circuit that synchronizes growth and maturation revealed through dilp8 binding to lgr3. *Science* **350**, aac6767 (2015).
- [8] Tataroglu, O. & Emery, P. Studying circadian rhythms in drosophila melanogaster. *Methods* **68**, 140–150 (2014).
- [9] Schindelin, J. *et al.* Fiji: an open-source platform for biological-image analysis. *Nature methods* **9**, 676–682 (2012).
- [10] Seong, K.-H., Matsumura, T., Shimada-Niwa, Y., Niwa, R. & Kang, S. The drosophila individual activity monitoring and detection system (diamonds). *Elife* **9**, e58630 (2020).
- [11] Ruf, F., Fraunholz, M., Öchsner, K., Kaderschabek, J. & Wegener, C. Weclmon—a simple and robust camera-based system to monitor drosophila eclosion under optogenetic manipulation and natural conditions. *PLoS One* **12**, e0180238 (2017).
- [12] Panadeiro, V., Rodriguez, A., Henry, J., Wlodkowic, D. & Andersson, M. A review of 28 free animal-tracking software applications: current features and limitations. *Lab animal* **50**, 246–254 (2021). Publisher: Nature Publishing Group US New York.
- [13] Gal, A., Saragosti, J. & Kronauer, D. J. antrax, a software package for high-throughput video tracking of color-tagged insects. *Elife* **9**, e58145 (2020).
- [14] Branson, K., Robie, A. A., Bender, J., Perona, P. & Dickinson, M. H. High-throughput ethomics in large groups of drosophila. *Nature methods* **6**, 451–457 (2009).
- [15] Romero-Ferrero, F., Bergomi, M. G., Hinz, R. C., Heras, F. J. & De Polavieja, G. G. Idtracker. ai: tracking all individuals in small or large collectives of unmarked animals. *Nature methods* **16**, 179–182 (2019).
- [16] Risse, B. *et al.* Fim, a novel ftir-based imaging method for high throughput locomotion analysis. *PloS one* **8**, e53963 (2013).
- [17] Berh, D. *et al.* An fim-based long-term in-vial monitoring system for drosophila larvae. *IEEE Transactions on Biomedical Engineering* **64**, 1862–1874 (2016).
- [18] Geissmann, Q. *et al.* Ethoscopes: An open platform for high-throughput ethomics. *PLoS biology* **15**, e2003026 (2017).
- [19] Mathis, A. *et al.* Deeplabcut: markerless pose estimation of user-defined body parts with deep learning. *Nature Neuroscience* (2018). URL <https://www.nature.com/articles/s41593-018-0209-y>.

- [20] Dominguez, M., Santoro, R., Rodriguez, V., Matic, A. & Greco, S. Flygear: Automated developmental time tracking system. URL <https://flygear.info/>.
- [21] Santoro, R. *The neural control of body symmetry, and an automated high-resolution pupae counting device*. Ph.D. thesis, Miguel Hernández University of Elche (2023). URL <https://hdl.handle.net/11000/32132>.
- [22] Santoro, R. Automated high-resolution pupae counting device (2023). European Patent Office, EP4238412.
- [23] Kyriacou, C. & Burnet, B. Genetic analysis of phototaxis near the upper limit of the visual spectrum of drosophila melanogaster. *Behavior Genetics* **9**, 123–128 (1979).
- [24] Wang, C.-Y., Bochkovskiy, A. & Liao, H.-Y. M. *Yolov7: Trainable bag-of-freebies sets new state-of-the-art for real-time object detectors*, 7464–7475 (2023).
- [25] Geissmann, Q., Rodriguez, L. G., Beckwith, E. J. & Gilestro, G. F. Rethomics: An R framework to analyse high-throughput behavioural data. *PLOS ONE* **14** (2019). Publisher: Public Library of Science.
- [26] Ryder, E. *et al.* The drosdel collection: a set of p-element insertions for generating custom chromosomal aberrations in drosophila melanogaster. *Genetics* **167**, 797–813 (2004).
- [27] Konopka, R. & Benzer, S. Clock mutants of drosophila melanogaster. *PNAS* **68**, 2112–2116 (1971).
- [28] Scargle, J. D. Studies in astronomical time series analysis. ii-statistical aspects of spectral analysis of unevenly spaced data. *Astrophysical Journal, Part 1, vol. 263, Dec. 15, 1982, p. 835-853*. **263**, 835–853 (1982).
- [29] Pereira, T. D., Shaevitz, J. W. & Murthy, M. Quantifying behavior to understand the brain. *Nature neuroscience* **23**, 1537–1549 (2020).
- [30] Reiser, M. The ethomics era? *Nature methods* **6**, 413–414 (2009).
- [31] Ogueta, M. & Garcia Rodriguez, L. Open source led controller for circadian experiments. *bioRxiv* 201087 (2017).
- [32] libcamera authors. libcamera: A complex camera support library for linux, android, and chromeos. URL <https://libcamera.org/>.
- [33] authors, Z. Zeromq: An open-source universal messaging library. URL <https://zeromq.org/>.
- [34] Stark, T. *et al.* Yolo object detection models can locate and classify broad groups of flower-visiting arthropods in images. *Scientific Reports* **13**, 16364 (2023).

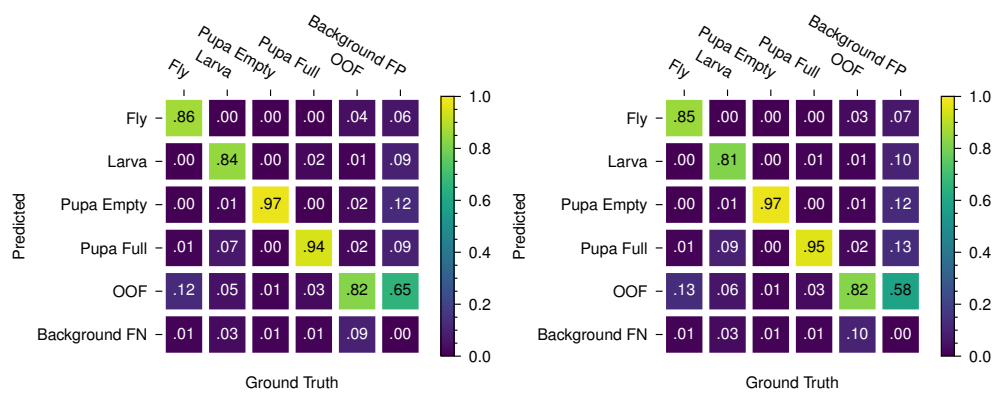
- [35] Ragab, M. G. *et al.* A comprehensive systematic review of yolo for medical object detection (2018 to 2023). *IEEE Access* (2024).
- [36] Lin, T.-Y. *et al.* *Microsoft coco: Common objects in context*, 740–755 (Springer, 2014).
- [37] developers, O. R. Onnx runtime (2021). URL <https://onnxruntime.ai/>.
- [38] Kuhn, H. W. The hungarian method for the assignment problem. *Naval research logistics quarterly* **2**, 83–97 (1955).
- [39] Riesen, K. & Bunke, H. Approximate graph edit distance computation by means of bipartite graph matching. *Image and Vision computing* **27**, 950–959 (2009).

Extended Data A YOLOv7 evaluation



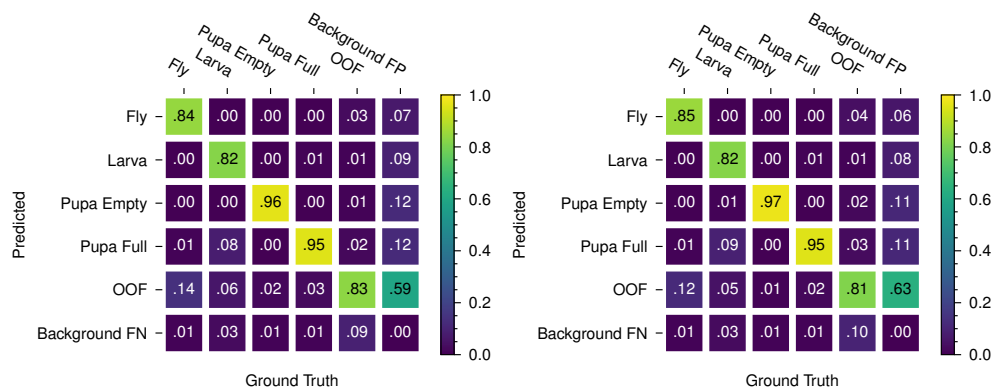
(a) YOLOv7-tiny

(b) YOLOv7



(c) YOLOv7-X

(d) YOLOv7-E6



(e) YOLOv7-W6

(f) YOLOv7-E6E

Fig. A1: Confusion matrices of YOLO models.

Extended Data B Bill of Material

Name	Model/Material	Vendor
Main Compartement		
Box	Spelsberg TK 3625 Grey	https://www.rs-online.com
3mm Acrylic base plate	PERSPEX Frost Midnight	https://www.expresszuschnitt.de
black matte	S2 9221	
Infrared filter	LUXACRYL-IR 3mm	https://www.go-tvv.com
2x Infrared filter clamp	3D printed, black PLA	
Vial Holder	3D printed, white PLA	
3x M4 12mm	A 2	https://www.theo-schrauben.de
Light Guide Panel		
Light guide panel	Acrylic Transparent 10mm	
2x Light guide panel clamp	3D printed, black PLA	
Diffuser sheet		
Infrared LEDs	SOLAROX LED IR 850NM IR1-60-850	https://www.led1.de
White LEDs	SOLAROX LED White	https://www.led1.de
2 core cable, 1m	RS PRO Control Cable, 2 Cores, 0.75mm ²	https://www.rs-online.com
Imaging		
Camera Holder	Acrylic/3D printed	
Raspberry Pi camera HQ		https://www.reichelt.com
Basler Lens	Basler C125-0818-5M-P	https://www.rauscher.de
Basler Spacer Ring CS-Mount	5mm	https://www.rauscher.de
Basler filter adapter	6/8mm	https://www.rauscher.de
Basler lens filter	MIDOPT LP818-46	https://www.rauscher.de
1x Aluminium profile	Type B Slot 6mm, 20x20x110mm	https://aluprofile24.de
1x T-Slot Nut 6mm	A 2	https://aluprofile24.de
2x M3 (10mm max)	A 2	https://www.theo-schrauben.de
4x M2 (20mm)	A 2	https://www.theo-schrauben.de
4x M2 Nut	A 2	https://www.theo-schrauben.de
Computing Hardware		
Raspberry Pi 4	8 GB	https://www.reichelt.com
Arduino Uno		https://www.reichelt.com
Arduino Nano 33 BLE Sense		https://www.reichelt.com
Mosfet/Light Controller	Custom Shield/Arduino IRF520 MOSFET Driver Module	
External brightness sensor	GY-302 BH1750	https://www.reichelt.com
USB A →USB B		https://www.rs-online.com
USB A →Mini-USB		https://www.rs-online.com
1x M4 Screw	A 2	https://www.theo-schrauben.de
8x M3 7mm	A 2	https://www.theo-schrauben.de
8x M3 Spacers 3mm	A 2	https://www.theo-schrauben.de
Ethernet Cable		https://www.rs-online.com
Network Switch		https://www.rs-online.com

Fig. B2: List of used materials.

Extended Data D Light guide panel design

For the light guide panel of the Hatching-Box we use 10mm thick acrylic glass with dimensions 93mm \times 220mm which was engraved with a pattern of circular carvings to distribute the light homogeneously. We provide a script for automatically generating a carving pattern based on minimal diameter of the carvings (d_{min}) and their minimal distance between each other (dst_{min}) in millimeter.

Extended Data E Automatic detection of vials

Based on a captured sample image we first transform the pixelwise grayscale intensity in the image of dimensions $W \times H$ to a linear signal $I(x)$ ($0 < x < W$) by applying a columnwise mean. We then calculate the derivative of $I(x)$ convolving the signal with the Sobel filter $S = [-2 \ 0 \ -2]$ to identify the most prominent changes in greyscale. Of the resulting values $D_I(x)$ we only keep those values for which applies

$$\hat{D}_I = \{D_I(x) | D_I(x) > \lambda \max_{0 < x < W} D_I(x)\} \quad (\text{E1})$$

with $0 < x < W$ and configurable λ . We achieved best results with $\lambda = 0.1$. Values in \hat{D}_I are sorted in descending order and further filtered by our prior knowledge of the object's dimensions in the image, e.g. rearing vials in the images are at least 1000 pixels wide, the gaps in between at least 200 pixels.